Breathable Polymer Films Produced by the Microlayer Coextrusion Process

CHAD MUELLER,[1] VASILY TOPOLKARAEV,[2] DAVE SOERENS,[2] ANNE HILTNER,[1] ERIC BAER[1]

[1] Department of Macromolecular Science and Center for Applied Polymer Research, Case Western Reserve University, Cleveland, Ohio 44106-7202

[2] Kimberly-Clark Corporation, Neenah, Wisconsin 54956

Received 19 November 1999; accepted 1 February 2000

ABSTRACT: Fabrication of a breathable film by the microlayer coextrusion process is described. Poly(ethylene oxide) (PEO) was microlayered with a filled polyolefin, either $CaCO_3$-filled polyethylene or $CaCO_3$-filled polypropylene. The thickness of individual layers was varied by increasing the total number of layers in the microlayered film from 8 to 4096. The water vapor transport rate (WVTR) was measured for microlayer films that varied in composition and number of layers. Especially with the PP($CaCO_3$)/PEO system, systematic variation in composition and number of layers made it possible to obtain large changes in the WVTR. The results were related to the tortuousity of the pathway through the microlayer. The filled polyolefins acted as a barrier to water vapor transport through the hydrophilic PEO. As the individual layers were made thinner by increasing the total number of layers, the polyolefin layers changed from continuous to discontinuous. Tortuousity concepts were used to correlate the increase in WVTR with an effective aspect ratio of the discontinuous polyolefin layers. In addition to high WVTR values, the breathable films produced by microlayering PEO with a filled polyolefin exhibited excellent mechanical properties. © 2000 John Wiley & Sons, Inc. J Appl Polym Sci 78: 816–828, 2000

Key words: breathable films; microlayer coextrusion; water vapor transport; filled polypropylene; filled polyethylene, Poly(ethylene oxide)

INTRODUCTION

Numerous examples in the literature illustrate how the coextrusion of film with two or more polymers into layered structures can produce films with a desirable mix of end-use characteristics. For packaging materials, laminates of polymers are used to provide various desirable properties such as oxygen barrier, water barrier, UV barrier, strength, puncture resistance, and heat sealability that one polymer by itself is not able to provide.[1]

Blend films with laminar morphologies are an alternative to coextruded films as barrier materials.[2–12] An example of such a material is a PP matrix containing dispersed laminar phases of EVOH, a high-barrier polymer, which had permeability properties approaching those of a multilayer coextruded system.[5,8] The key to achieving good barrier with these materials is creating impermeable domains with high aspect ratios perpendicular to the transport direction. This creates a torturous path, which the permeant must traverse to pass through the thickness of the film. Films that have this laminar morphology can

Correspondence to: A. Hiltner.
Contract grant sponsor: Kimberly-Clark Corp.

Journal of Applied Polymer Science, Vol. 78, 816–828 (2000)

have very novel properties. By varying the aspect ratio of the barrier domains it is possible to tailor the permeability of the film. The permeable material remains continuous in the thickness of the film, but the aspect ratio of the barrier domains controls the tortuousity and hence the permeability of the film.

An interesting variation of the laminar morphology is a three-dimensionally cocontinuous structure of PTFE and silicone elastomer described by Dillon.[13] This is a semiinterpenetrating polymer network (semi-IPN) of microporous PTFE and silicone elastomer. The porosity is controlled by the stretching conditions during processing, and the surface energy is controlled by the composition. Thus, it is possible to control the permeability of these structures. The continuous silicone phase lends the structure permeability, while the continuous PTFE phase provides mechanical properties. This is a unique system because it can be a liquid barrier while remaining permeable to gases and water vapor. Examples of uses for this type of material are as wound dressings, barrier textiles,and filtration systems.

With such a cocontinuous system, one of the continuous phases can provide good mechanical properties while the other continuous phase can provide a pathway for permeation. The permeability of such a system would then depend on the tortuousity of the permeable phase. Cocontinuous blends are usually limited in their composition range, and the morphology is highly dependent on the mixing conditions.[14] It would be desirable to control the tortuousity to tailor the permeability, but this is often not possible.[15]

Microlayer coextrusion offers an alternative method for creating semipermeable films. The microlayer coextrusion process is typically used to combine dissimilar polymers to make useful structures that synergistically combine the properties of the materials.[1,16–18] When the layers become very thin, instabilities occur and the layers begin to break up. As the layers break up, the film becomes continuous through its thickness as well. With a small number of relatively thick, essentially continuous layers, this system would have an extremely torturous pathway through its thickness, but as the number of layers increases and individual layers become very thin, layer breakup would decrease the tortuosity. By combining a permeable polymer and an impermeable polymer in this process, a semipermeable film with tailorable permeability properties could be produced.

One such interesting candidate material for this microlayer coextrusion process is poly(ethylene oxide) (PEO), a water-soluble polymer. The hydrophilicity of PEO makes it water vapor breathable and absorbent. However, by itself, PEO does not have sufficient mechanical properties. The goal of this work was to microlayer PEO with suitable materials to improve the mechanical properties while maintaining a high level of breathability. Linear low-density polyethylene (LLDPE) and polypropylene (PP) were selected as candidates to improve the mechanical properties. Because LLDPE and PP are both barriers to water vapor, $CaCO_3$ particles were added to create pathways for water vapor transport through the polyolefin layers. It was thought that when the polyolefin layer thickness approached the $CaCO_3$ particle size (nominally 1 μm), the particles would cut through the layers and provide a pathway for water vapor.

Microporous structures have previously been created by stretching films with $CaCO_3$ or another filler to create microvoids around the particles.[19–24] Permeability measurements are a useful probe for characterizing the heterogeneous morphology.[25,26] In this work, water vapor transport rate (WVTR) was used to probe the morphologies that were obtained with the microlayer process. Mechanical tests were also used to determine the effect of the polyolefin in reinforcing the microlayer films.

MATERIALS AND METHODS

Materials

Polymers for microlayer coextrusion were provided in the form of pellets by Kimberly-Clark. Poly(ethylene oxide) (PEO) with a weight-average molecular weight of 400,000 was used. PEO is water soluble and semicrystalline, with a melting temperature of 65°C. Three types of polyethylene were provided: a linear low-density polyethylene (Dowlex NG) denoted as PE, PE with 50 wt % calcium carbonate denoted as PE($CaCO_3$), and PE with 45 wt % calcium carbonate and 5 wt % silicone glycol additive denoted as PE($CaCO_3$ + SG). A polypropylene with 60 wt % calcium carbonate denoted as PP($CaCO_3$) was also provided. The $CaCO_3$ particles were nominally 1 μm in diameter. The resins were processed in the as-received condition except for PE($CaCO_3$ + SG), which was

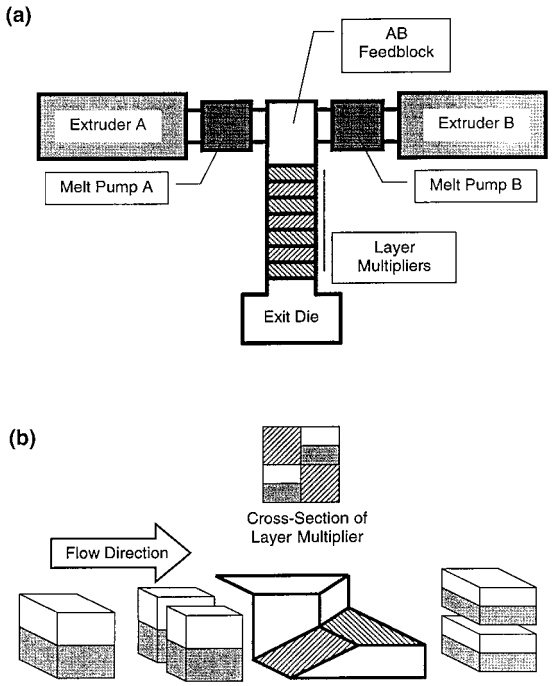

Figure 1 Schematic representation of the two-component microlayer coextrusion system: (a) arrangement of system components, and (b) cutting, spreading, and recombining of the melt stream by a multiplier element to double the number of layers.

dried overnight at 80°C under vacuum prior to extrusion.

The viscosity of each material was determined as a function of temperature using a Kayeness Galaxy 1 melt flow indexer. The shear rate during melt indexing ranged from 1 to 4 s^{-1}. The melt flow rate was measured according to ASTM D1238-90B, and the viscosity was calculated as the shear stress at the wall divided by the shear rate at the wall.

Microlayer Coextrusion

The microlayer coextrusion system consisted of two three-quarter inch single screw extruders with melt pumps, an AB type coextrusion feedblock, a series of layer multiplier elements, and a 15-cm film die [Fig. 1(a)]. This system has been described previously, and has been used to produce other polymer microlayer systems.[16,17] Metering pumps controlled the two melt streams that were combined in the feedblock as two parallel layers. From the feedblock, the two layers flowed through a series of layer multiplying elements; each element doubling the number of layers. In each element, the melt was first sliced vertically, then spread horizontally, and finally recombined [Fig. 1(b).] An assembly of n multiplier elements produced an extrudate with the layer sequence $(AB)_x$ with x equal to 2^n. The film was cast onto a chill roll to produce 1 mil (25 μm) thick films about 10 cm wide. Microlayer samples were produced over the entire composition range by varying the volumetric ratio of the melt streams with the melt flow pumps.

The composition of microlayers containing $CaCO_3$ were analyzed by thermogravimetric analysis (TGA). A Perkin-Elmer TGA 7 was used to determine the weight of $CaCO_3$ remaining after the temperature was ramped from ambient to 700°C at a rate of 20°C/min. A mixture of nitrogen and oxygen was used in the furnace of the TGA. Specimens were cut from the center third of each film and stacked in the sample pan to achieve an initial weight of 510 mg.

Water Vapor Transport Rate

The water vapor transport rate (WVTR) was measured by a modified ASTM E96-93 method. The film covered a Petri dish filled with distilled H_2O as shown schematically in Figure 2. The mass of H_2O lost from the dish was monitored as a function of time, and a water vapor transport rate was obtained from the steady-state region. Specimens were cut from the center of the films, and thickness measurements in a minimum of five locations on the specimen were performed using a dial gauge. Standard deviation in the thickness of individual specimens was typically less than 10%. Specimens were selected so that the thickness was as close to 1 mil as possible. A 5 × 5-cm window was cut in a sheet of aluminum foil and the film was attached to the aluminum with 5 Minute® Epoxy (Devcon). The aluminum foil mask containing the film was attached to the top of a plastic Petri dish with epoxy. Using a syringe, 20–30 mL of distilled H_2O was added to the Petri

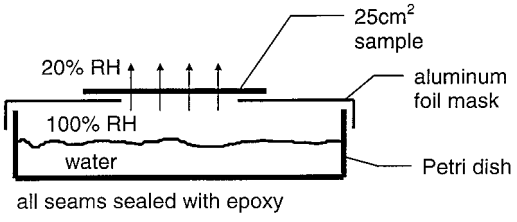

Figure 2 Schematic of the test cell used to measure WVTR.

dish and the hole was sealed with epoxy. Specimens were attached with the polyolefin surface facing the H_2O. After allowing the epoxy to cure for an hour, the specimens were weighed and placed in a convection oven at 40°C and 15–20%RH. The specimens were periodically removed from the oven and weighed. Other specimens with testing areas from 7 to 25 cm^2 were tested to determine the effect of area on WVTR. To test the limits of this method of measuring WVTR, a specimen with no polymer film in place and a specimen with aluminum foil in place of the polymer film were tested. The open test cell lost water at the rate of 61 g/day compared to about 10 g/day for the PEO control, which had the highest measured WVTR. The closed test cell lost water at the rate of 0.2 g/day, which was comparable to the samples with the lowest WVTR values. Film samples with these WVTR values were considered as being barriers to water vapor.

Film Characterization

Uniaxial stress–strain measurements were performed using an Instron model 1122 universal testing machine. Microtensile specimens were cut in the extrusion direction from the center of the film, and thickness measurements were performed with a film gauge. Tests were made at ambient temperature with a strain rate of 50%/min.

Films were examined in cross-section using scanning electron microscopy (SEM). To prepare the cross-sections, the films were cryofractured in liquid nitrogen. The PEO was sometimes removed from the cryofractured surface by washing in ethanol. The films were coated with 90 Å gold and examined using an SEM (JEOL–JSM 840A).

RESULTS AND DISCUSSION

Microlayer Processing

In producing microlayer films, large differences in viscosity of the two components can lead to a number of instabilities during coextrusion.[1] The viscosities of the various polyethylene resins are compared with the PEO viscosity in Figure 3. Using this plot, the extrusion conditions for each PE/PEO pair were selected so that the viscosities would be matched as closely as possible. The PEO was extruded at 150°C, PE at 190°C, PE($CaCO_3$) at 190°C, and the PE($CaCO_3$ + SG) at 170°C. The

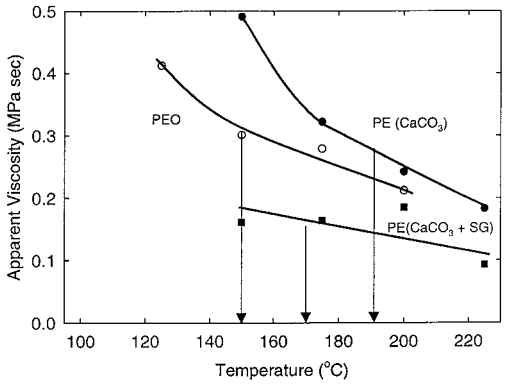

Figure 3 Viscosity of PEO and filled polyethylenes. The arrows indicate the extruder temperatures used for microlayer coextrusion.

feedblock, layer multipliers, adapter, and exit die were set to the temperature of the particular PE that was being extruded. The components were microlayered with the two-component system that has been previously described.[16,17] A 15-cm film die and chill roll were used to produce films as close to 1 mil thick as possible. Table I lists the composition and number of layers of the PE-($CaCO_3$ + SG)/PEO films that were extruded.

As with the polyethylene systems, the viscosities of the PP($CaCO_3$) and PEO were compared to determine the processing temperatures with the best viscosity match (Fig. 4). The PEO was extruded at 150°C, the PP($CaCO_3$) was extruded at 220°C, and the feedblock, layer multipliers, adapter, and exit die were set to 220°C. A 15-cm film die and chill roll were used to produce films with thicknesses as close to 1 mil as possible. Table II lists the composition and number of layers of the PP($CaCO_3$)/PEO films that were extruded.

The composition of each PE($CaCO_3$ + SG)/PEO microlayer sample was determined by TGA. Decomposition began at about 200°C and was complete at 400–450°C. The weight fraction remaining after decomposition was taken as the weight fraction $CaCO_3$ in the microlayer. The microlayer PE($CaCO_3$ + SG) control film was determined to contain 44 wt % $CaCO_3$. To calculate the weight and volume fraction of PE($CaCO_3$ + SG) in microlayers with PEO, the PE($CaCO_3$ + SG) was assumed to contain 44 wt % $CaCO_3$, and density values of 0.92 and 2.71 g/cc were used for LLDPE and $CaCO_3$, respectively. The PEO weight fraction and volume fraction were then calculated using a PEO density value of 1.15 g/cc.[27] The expected and measured volume compositions of

Table I Composition of PE($CaCO_3$ + SG)/PEO Microlayer Films Determined by TGA

Number of Layers	PE($CaCO_3$ + SG)/PEO Ratio as Extruded (vol/vol)	$CaCO_3$ Content by TGA (wt %)	PE($CaCO_3$ + SG)/PEO Ratio Calculated from TGA (vol/vol)
PE($CaCO_3$ + SG) Microlayer		44.0	
8	10/90	4.4	9/91
	30/70	13.1	27/73
	50/50	23.6	51/49
16	10/90	5.4	11/89
	30/70	17.1	36/64
	50/50	26.4	57/43
256	30/70	25.8	56/44
	50/50	25.0	54/46
	60/40	26.2	57/43
	70/30	29.8	65/35
512	30/70	16.5	35/65
	50/50	21.2	45/55
1024	5/95	7.5	15/85
	10/90	11.9	25/75
	20/80	13.0	27/73
	30/70	18.0	38/62
	50/50	28.2	61/39
	70/30	31.6	69/31

the PE($CaCO_3$ + SG)/PEO microlayers are compared in Table I. The microlayers are identified by the PE($CaCO_3$ + SG)/PEO volume ratios expected from the extrusion conditions; however, when data are plotted as a function of composition, the actual PE($CaCO_3$ + SG)/PEO volume ratios determined by TGA are used.

Compositions of the PP($CaCO_3$)/PEO microlayers were determined in a similar manner. The microlayer PP($CaCO_3$) control film was found to contain 60 wt % $CaCO_3$, and the PP density was assumed to be 0.90 g/cc. The expected and measured compositions of the PP($CaCO_3$)/PEO microlayers are shown in Table II. As with the PE($CaCO_3$ + SG)/PEO microlayers, the PP($CaCO_3$)/PEO microlayers are identified by the volume ratios expected from the extrusion conditions; however, when data are plotted as a function of composition, the actual PP($CaCO_3$)/PEO volume ratios determined by TGA are used.

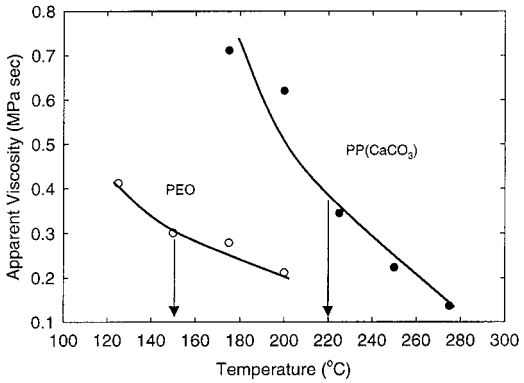

Figure 4 Viscosity of PEO and filled PP. The arrows indicate the extruder temperatures used for microlayer coextrusion.

Table II Composition of PP($CaCO_3$)/PEO Microlayer Films Determined by TGA

Number of Layers	PP($CaCO_3$)/PEO Ratio as Extruded (vol/vol)	$CaCO_3$ Content by TGA (wt %)	PP/PEO Ratio Calculated from TGA (vol/vol)
PP($CaCO_3$) Microlayer		60.0	
256	10/90	12.2	16/84
	30/70	31.0	45/55
	50/50	37.2	55/45
1024	10/90	8.9	12/88
	30/70	22.2	31/69
	50/50	39.9	60/40
4096	10/90	9.4	12/88
	30/70	22.5	31/69
	50/50	35.1	52/48

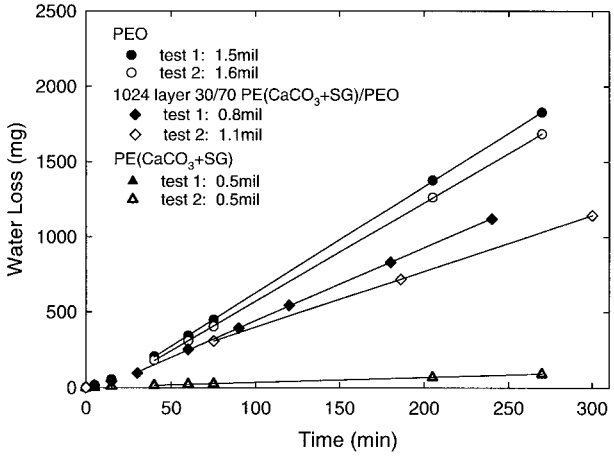

Figure 5 Typical test cell measurements of water loss as a function of time for microlayered films. The WVTR was obtained from the linear portion of the plot.

Water Vapor Transport Rate of Microlayers with Polyethylene

The water vapor transport rate (WVTR) was measured under identical conditions of temperature and relative humidity for all specimens. The measured water loss as a function of time for representative tests of the microlayer controls and a PE($CaCO_3$ + SG)/PEO microlayer film is shown in Figure 5. The rate of water loss was linear with time after an initial period of about 45–60 min. This initial period was attributed to temperature and humidity equilibration in the specimen dish. Most WVTR tests were run for 3–4 h after tests to 24 h verified that 3–4 h was sufficient to achieve steady state. The slope of the water loss vs. time was normalized to the testing area. Because the thickness of the film specimens varied, it was also necessary to normalize to thickness:

$$\text{WVTR} = \frac{\text{mass } H_2O \text{ lost}}{\text{time} \times \text{area}} \times \text{thickness} \qquad (1)$$

with units of g mil/day/m^2. The assumption that WVTR was inversely proportional to the film thickness was not tested in this study.

Microlayer specimens of 1024 layer 30/70 PE-(CaCO3 + SG)/PEO with areas ranging from 25 to 7 cm^2 were tested to determine if there was any effect of testing area on the WVTR. The WVTR did not vary over this area range, and all subsequent WVTR tests were performed with a specimen area of 25 cm^2.

Because PEO is a water soluble polymer, it had a very high WVTR. When normalized to thickness and area, the WVTR of PEO was 6220 ± 350 g mil/day/m^2. The PE($CaCO_3$ + SG) microlayer control was nearly impermeable to water vapor with a WVTR of 100 ± 1 g mil/day/m^2. Values of WVTR for all the microlayer control films with and without normalization to thickness are tabulated in Table III. All of the polyolefin films were barriers to water vapor.

The WVTR values as a function of composition for PE($CaCO_3$ + SG)/PEO microlayer films with different number of layers are shown in Figure 6. The WVTR of microlayers with 8 and 16 layers remained low, less than 100 g mil/day/m^2, until the PEO content exceeded 80%. In contrast, microlayers with 256, 512, and 1024 layers showed a higher WVTR that increased with increasing PEO content.

For two components combined as microlayers, the limits of the WVTR are predicted by the rule of mixtures for the parallel and series cases.[28] The series case describes the WVTR through continuous layers of the components arranged perpendicular to the transport direction. In this case, the WVTR is given by:

$$\frac{1}{\text{WVTR}} = \frac{\Phi_a}{\text{WVTR}_a} + \frac{\Phi_b}{\text{WVTR}_b} \qquad (2)$$

Table III Water Vapor Transport Rate of Microlayer Control Films

Sample	Thickness (mils)	WVTR (g/day/m^2)	WVTR Normalized to Thickness (g mil/day/m^2)
PEO	1.6 ± 0.1	3890 ± 220	6220 ± 350
PE	1.2 ± 0.1	50 ± 1	60 ± 1
PE($CaCO_3$)	1.4 ± 0.1	50 ± 1	70 ± 1
PE($CaCO_3$ + SG)	0.5 ± 0.1	190 ± 1	100 ± 1
PP($CaCO_3$)	1.0 ± 0.1	20 ± 1	20 ± 1

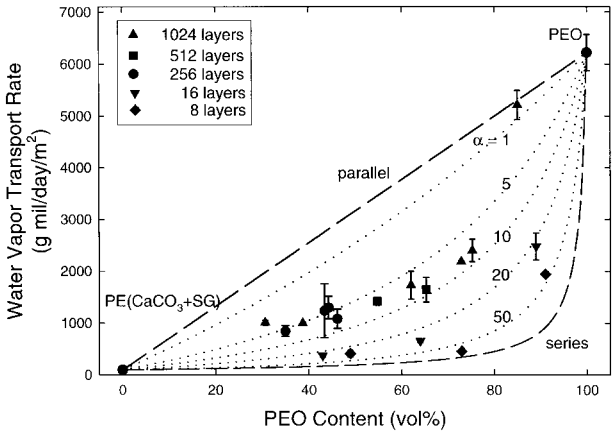

Figure 6 Effect of composition on the WVTR of PE($CaCO_3$ + SG)/PEO microlayer films. The dotted lines are from eq. (6).

where Φ_a and Φ_b are the volume fractions of the respective components. For the other case where the continuous layers are parallel to the transport direction, the WVTR is given by:

$$\text{WVTR} = \Phi_a \text{WVTR}_a + \Phi_b \text{WVTR}_b \qquad (3)$$

These models provided lower and upper bounds for the data in Figure 6. The series model nearly fit the 8 and 16 layer data, indicating that these microlayer films had nearly continuous layers of PE($CaCO_3$ + SG) that acted as barriers to water vapor. The 256, 512, and 1024 layer films had WVTR values that fell between the two limits defined by the rule of mixtures.

The morphology of eight-layer 30/70 PE($CaCO_3$ + SG)/PEO, which had a WVTR just slightly higher than that predicted by the series model, is shown in Figure 7. Eight continuous layers were discernable, with unfilled PEO layers visible between filled PE($CaCO_3$ + SG) layers. The thickness of the PE($CaCO_3$ + SG) layers approached the diameter of the particles. As individual layers were made thinner by increasing the number of layers, some of the particles would be large enough to cut through the polyolefin layers. By following particle boundaries and interstices, water vapor would have a continuous pathway through the polyolefin layers and, hence, through the thickness of the film.[29] As the number of layers increased further, it was anticipated that the layers would break up and the PEO phase would become continuous in the thickness of the film. These factors accounted for the gradually increasing WVTR with increasing number of layers.

The morphology of 1024 layer 30/70 PE($CaCO_3$ + SG)/PEO microlayer, which had a WVTR intermediate between the models, is also shown in Figure 7. The specimen was cryofractured and etched to remove the PEO. The morphology resembled that of a cocontinuous system. Discontinuous PE($CaCO_3$+ SG) layers provided evidence of numerous pathways for water vapor transport through the thickness of the film. If the PE($CaCO_3$ + SG) layers had been continuous for this sample, their thickness would have been 15 nm. Because of the viscosity mismatch and the presence of $CaCO_3$ particles, the layers broke up during the layer multiplication process.

The tortuousity model of Nielsen was used to describe the WVTR of films with discontinuous polyolefin layers.[30] Impermeable platelets distributed in a permeable matrix act as barriers to diffusion and increase the distance that the permeant must travel to pass through the film. The increase in distance is described by the tortuousity factor τ, defined as the distance a permeant molecule travels through the films divided by the film thickness. The tortuousity reduces the WVTR of the film as:

$$\text{WVTR}_{\text{filled}} = \frac{\text{WVTR}_{\text{matrix}} \Phi_{\text{matrix}}}{\tau} \qquad (4)$$

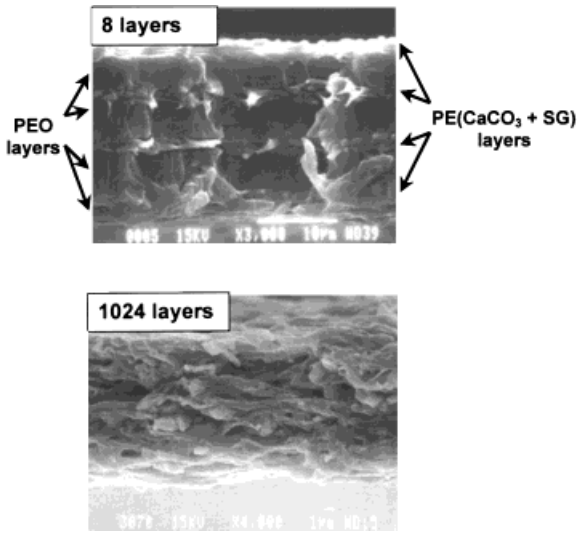

Figure 7 Scanning electron micrographs of cross-sections of 30/70 PE($CaCO_3$ + SG)/PEO microlayer films: eight layers with continuous polyolefin layers, and 1024 layers after etching to remove the PEO showing discontinuous polyolefin layers.

For platelet particles the tortuousity factor is given by:

$$\tau = 1 + \frac{L}{2W}\,\Phi_{\text{matrix}} \tag{5}$$

where L and W are the length and width of the platelets. Combining eqs. (4) and (5), the WVTR is given by:

$$\text{WVTR}_{\text{filled}} = \frac{\text{WVTR}_{\text{matrix}}\Phi_{\text{matrix}}}{1 + 0.5\alpha\Phi_{\text{matrix}}} \tag{6}$$

where α = L/W is the aspect ratio of the platelets.

In applying the tortuousity model to the PE-($CaCO_3$ + SG)/PEO microlayers, the PEO was treated as the permeable matrix, and the discontinuous PE($CaCO_3$ + SG) layers were treated as the impermeable platelets. The data for PE-($CaCO_3$ + SG)/PEO microlayers were compared to the predictions of eq. (6) for various values of α (Fig. 6). The data for 8 and 16 layers fell above the lower limit, with α values in the range of 20–50. Aspect ratios of this magnitude might result from larger $CaCO_3$ particles breaking through the polyolefin layer to create pathways in the thickness direction for transport of water vapor. The 256, 512, and 1024 layer WVTR data fell within a range of α values of 5–10. These α values were consistent with a film in which the PE($CaCO_3$ + SG) layers had broken up and permitted formation of a continuous PEO phase in the thickness direction.

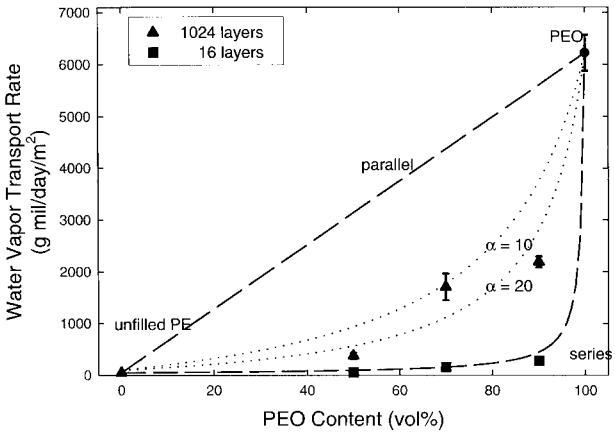

Figure 8 Effect of composition on the WVTR of 16 and 1024 layer PE/PEO microlayer films. For comparison, the dotted line fits to eq. (6) represent data for PE($CaCO_3$ + SG)/PEO microlayers with 16 (α = 20) and 1024 layers (α = 10).

Microlayer films of 50/50 PE($CaCO_3$)/PEO with 256 and 512 layers had slightly lower WVTR values than the comparable PE($CaCO_3$ + SG)/PEO films. The difference was attributed to the hydrophilicity of SG.[31]

Microlayers with unfilled PE layers were also tested. The WVTR for PE/PEO samples with 16 and 1024 layers is shown in Figure 8. The series model for continuous layers fit the 16 layer data very well, whereas the data for 16 layer PE-($CaCO_3$ + SG)/PEO films fit the tortuosity model, with an aspect ratio of about 20, indicating that the $CaCO_3$ particles had caused some disruption of the polyolefin layers. The difference in breathability between the unfilled and filled 16 layer films showed the importance of the $CaCO_3$ particles in creating pathways through the PE layer. The 1024 layer unfilled films also had lower breathability than the 1024 layer filled films. Whereas the filled films had α values of 5–10, the unfilled films were fit by an α value of 20. Apparently even though the polyolefin layers could not be broken up by filler particles, the unfilled PE layers underwent layer breakup when the layers became very thin giving these films improved breathability.

Water Vapor Transport Rate of Microlayers with Polypropylene

The WVTR of the PP($CaCO_3$)/PEO microlayers was also studied. As with the PE materials, PP-($CaCO_3$) was a barrier to water vapor with a WVTR of 20 ± 1 g mil/day/m^2. The WVTR of PP($CaCO_3$)/PEO microlayers in Figure 9 showed a clear effect of layer thickness with WVTR increasing as the number of layers increased. Data for microlayers with 256, 1024, and 4096 layers fit eq. (6), with α values of 20, 10, and 3, respectively. The aspect ratios were in the range consistent with the breakup of the PP($CaCO_3$) layers. The decrease in tortuousity with an increasing number of layers indicated that with this system, films with controlled permeability could be obtained with the microlayer process.

The morphology of the 30/70 PP($CaCO_3$)/PEO microlayers is shown in Figure 10. The structure was similar to that observed for PE($CaCO_3$ + SG)/PEO microlayers with discontinuous polyolefin layers. Although the WVTR of these samples nearly doubled from 256 to 1024 layers and doubled again with 4096 layers, differences in aspect

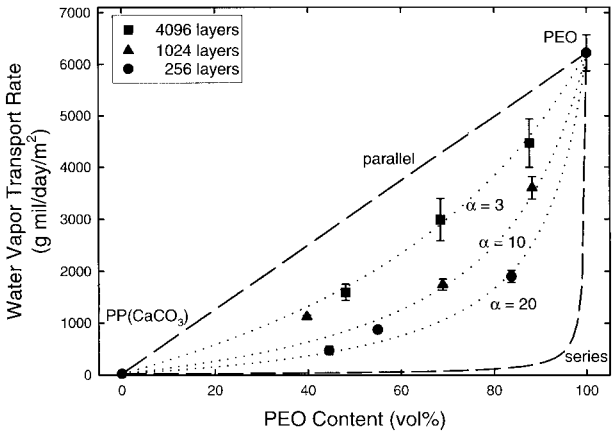

Figure 9 Effect of composition on the WVTR of PP-($CaCO_3$)/PEO microlayer films. The dotted lines are from eq. (6).

ratio of the polyolefin inferred from the WVTR measurements were not apparent in micrographs of the samples.

Based on the measured WVTR of the various PE/PEO and PP/PEO microlayer systems, the models for water vapor transport in Figure 11 were proposed. When the layers were thick enough, they remained continuous, and the WVTR followed the series model. This behavior was exemplified by 16-layer PE/PEO microlayers. If the polyolefin layer was filled with $CaCO_3$, the particles cut through the polyolefin layers when the layer thickness decreased to the size scale of the particles, thus giving water vapor a pathway through the otherwise essentially impermeable polyolefin layers. Although these samples, for example 16 layer PE($CaCO_3$ + SG)/PEO, had a higher WVTR than predicted by the series model, the relatively large α value from the Nielsen model indicated a high degree of tortuousity in the water vapor pathway. As the number of layers increased and the layer thickness decreased further, the layers broke up during processing and a continuous PEO pathway formed in the thickness direction. The WVTR was high because the water vapor traveled easily through the PEO phase. Especially with the PP($CaCO_3$)/PEO system, systematic variation in the structure with decreasing layer thickness made it possible to control the WVTR over a wide range between the predicted upper and lower bounds.

Mechanical Behavior of Polyethylene Microlayers

The PEO films necked and fractured during drawing without undergoing strain hardening. In contrast, PE($CaCO_3$ + SG) extended almost uniformly to much higher strains (Fig. 12). Microlayer films of 50/50 and 30/70 PE($CaCO_3$ + SG)/PEO retained some of the properties of the polyolefin, including increased fracture stress and elongation at fracture. Only when the polyolefin content was very low, as in the 10/90 PE($CaCO_3$ + SG)/PEO microlayer, did the mechanical properties resemble those of PEO.

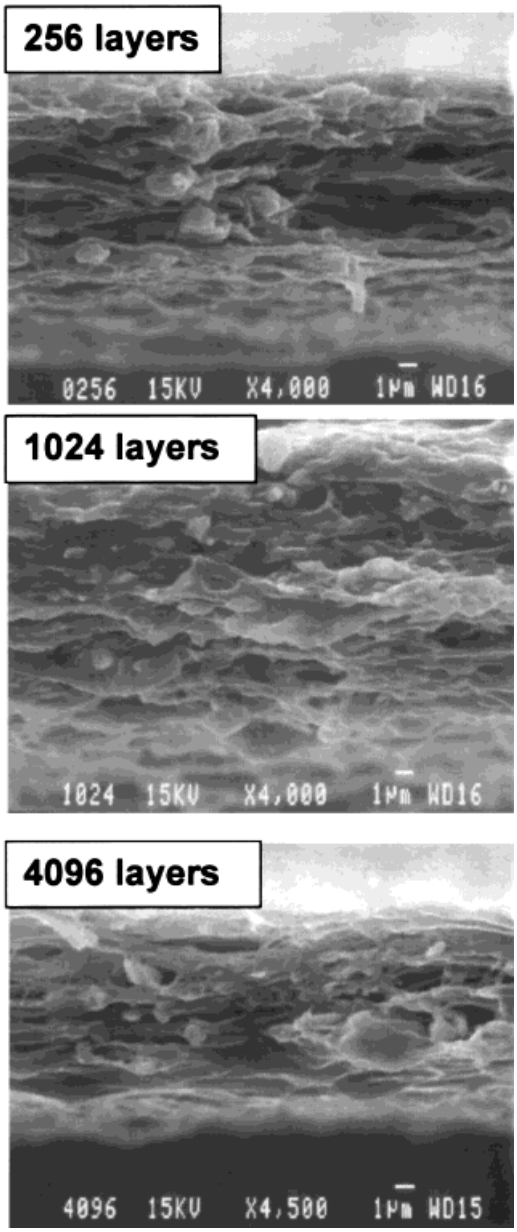

Figure 10 Scanning electron micrographs of cross-sections of the 30/70 PP($CaCO_3$)/PEO microlayer films after etching to remove the PEO: 256 layers, 1024 layers, and 4096 layers.

Modulus values of the various compositions are plotted in Figure 13(a). The PEO and PE($CaCO_3$ + SG) films had similar modulus values of about 100 MPa and 85 MPa, respectively. In addition to these two controls, modulus values of unfilled PE and PE($CaCO_3$) are included in Figure 13(a). Because the moduli of unfilled PE and PE($CaCO_3$ + SG) were about the same, and much lower than the modulus of PE($CaCO_3$), the $CaCO_3$ particles in the PE($CaCO_3$ + SG) were thought to be debonded and, therefore, did not contribute to increasing the modulus. The modulus values of the microlayers followed the additivity rule for continuous layers parallel to the stretch direction. In this property, the 8- and 16-layer microlayers with continuous polyolefin layers were not differentiated from the microlayers with a higher number of layers and discontinuous polyolefin layers.

The yield strength is compared in Figure 13(b). As with the modulus, films of PEO and PE($CaCO_3$ + SG) had similar yield strengths of 8 and 9 MPa, respectively. The fact that PE($CaCO_3$ + SG) and PE($CaCO_3$) had about the same yield strength as unfilled PE indicated that the $CaCO_3$ particles debonded prior to yielding in both cases. The yield strength of the PE($CaCO_3$ + SG)/PEO microlayers was essentially additive, and there was no significant effect of the number of layers.

The PE($CaCO_3$ + SG) film had a much higher fracture strength than the PEO film due to strain hardening. Microlayers of PE($CaCO_3$ + SG)/PEO with less than 80 vol % PEO exhibited some degree of synergy in the fracture strength with a positive deviation from the upper bound predicted by the rule of mixtures for continuous layers in the stretch direction. This was attributed to the microlayer morphology. The layers were thin enough that the polyolefin induced strain hardening in the PEO, which resulted in increased fracture strength. Microlayers with more than 80 vol % PEO did not exhibit strain hardening, and the fracture strength followed the rule of mixtures.

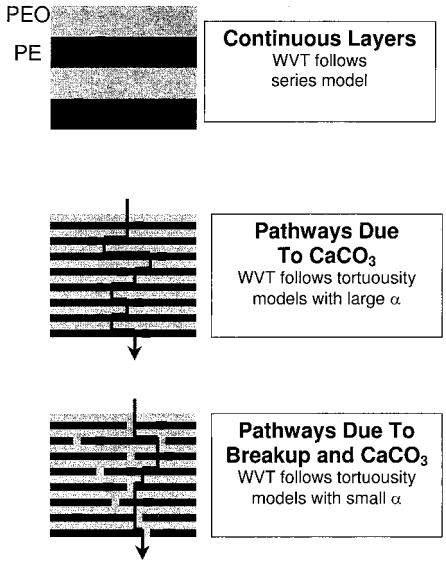

Figure 11 Schematic representation of the proposed models for water vapor transport in microlayer films.

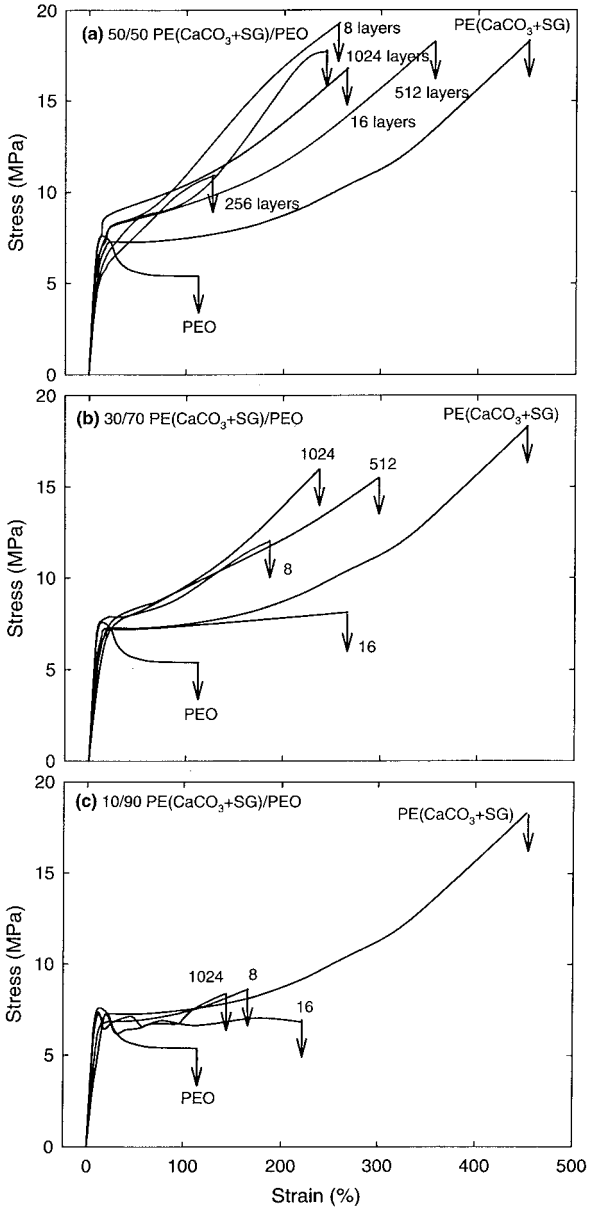

Figure 12 Effect of the number of layers on the stress–strain behavior of PE($CaCO_3$ + SG)/PEO microlayer films: (a) 50/50 composition, (b) 30/70 composition, and (c) 10/90 composition.

For the specific case of the 16-layer 30/70 composition, individual layers were observed to fracture during drawing. Specimens did not undergo strain hardening, which resulted in a reduced value of fracture strength. Synergistic fracture behavior has been observed in microlayers of other polymers as the thickness of individual layers is decreased, for example, in microlayers with filled and unfilled layers of PP[16,17] and with layers of PC and SAN.[18]

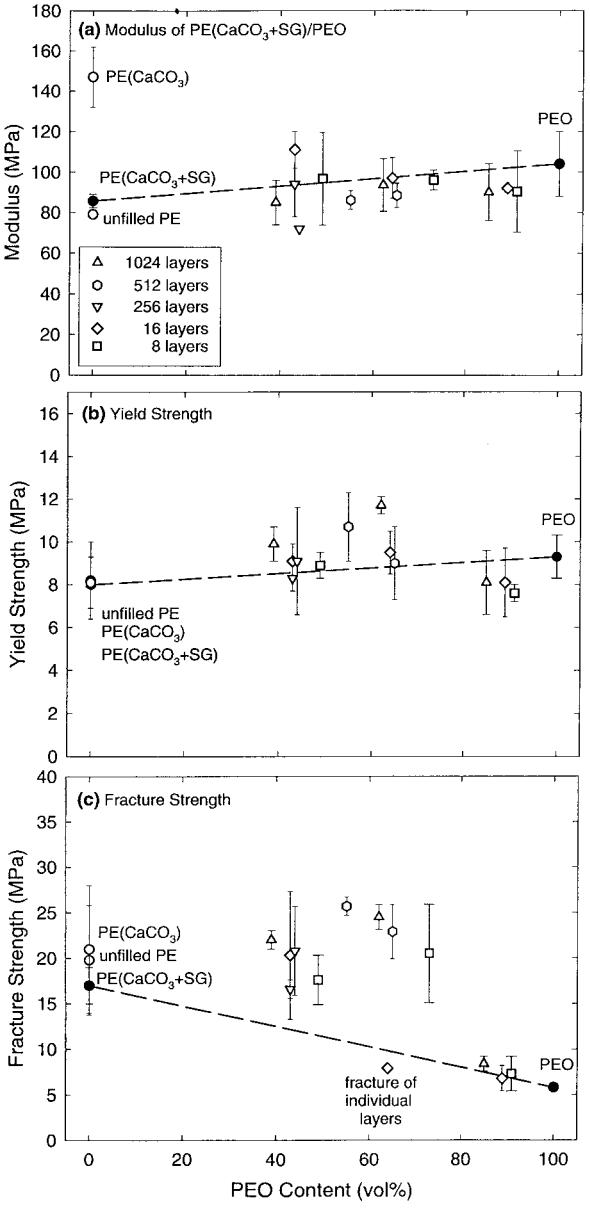

Figure 13 Effect of composition on the mechanical properties of PE($CaCO_3$ + SG)/PEO microlayer films: (a) modulus, (b) yield strength, and (c) fracture strength.

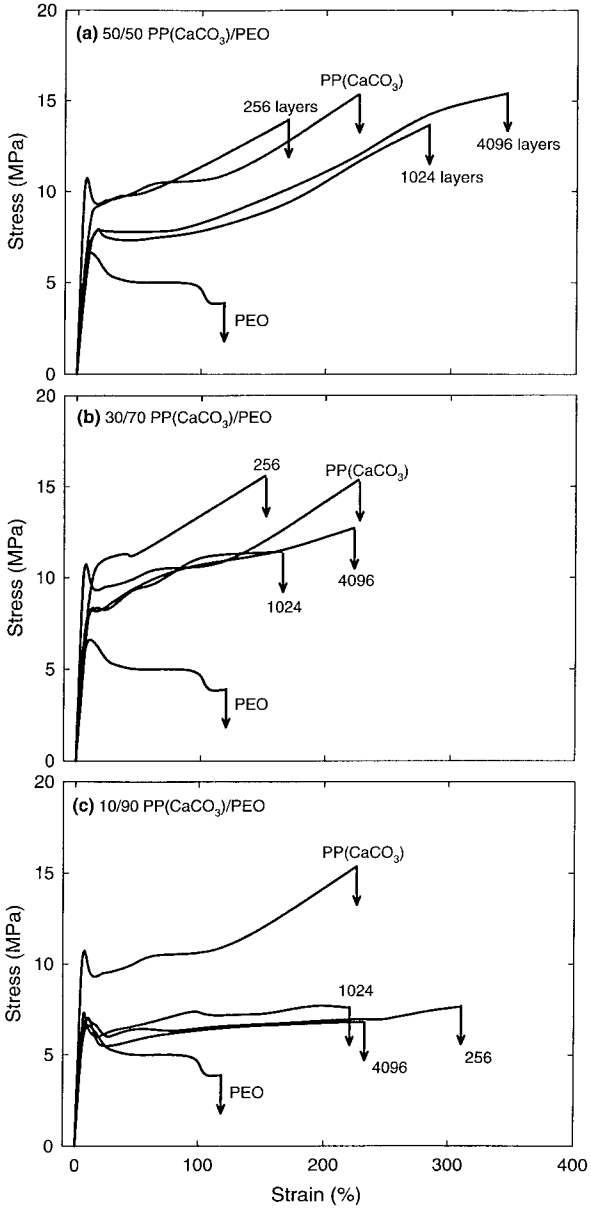

Figure 14 Effect of the number of layers on the stress–strain behavior of PP($CaCO_3$/PEO microlayer films: (a) 50/50 composition, (b) 30/70 composition, and (c) 10/90 composition.

Mechanical Behavior of Polypropylene Microlayers

Microlayering dramatically improved the toughness of PP($CaCO_3$)/PEO microlayers as shown in Figure 14 for the 50/50, 30/70, and 10/90 compositions. Whereas both PP($CaCO_3$) and PEO control films necked, deformation of the PP($CaCO_3$)/PEO microlayer films tended toward diffuse necking approaching homogeneous deformation. The 50/50 and 30/70 compositions strain hardened

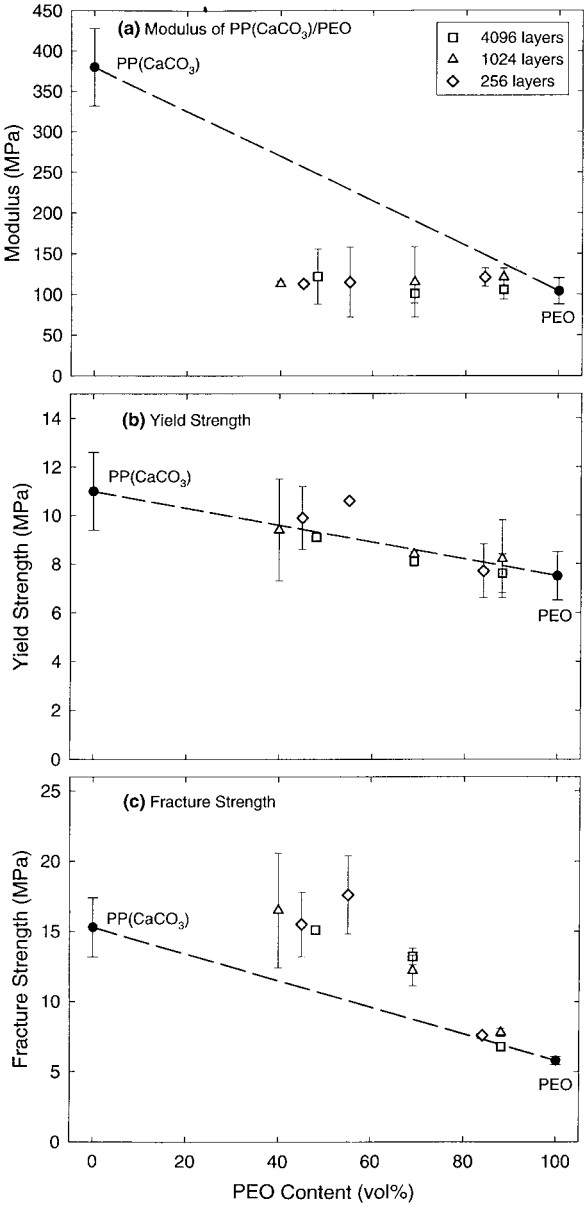

Figure 15 Effect of composition on the mechanical properties of $PP(CaCO_3)$/PEO microlayer films: (a) modulus, (b) yield strength, and (c) fracture strength.

prior to fracture; only the 10/90 composition fractured without strain hardening. However, all the $PP(CaCO_3)$/PEO microlayers including the 10/90 composition exhibited excellent ductility.

The modulus of 256, 1024, and 4096 layer $PP(CaCO_3)$/PEO microlayer films is plotted in Figure 15(a) as a function of composition. The $PP(CaCO_3)$ had a modulus almost four times greater than PEO, but the modulus of $PP(CaCO_3)$/PEO microlayer films was very similar to the PEO modulus, and below the lower bound predicted by the rule of mixtures for layers perpendicular to the stretch direction. A possible explanation for the unexpectedly low modulus of the microlayers was that the $CaCO_3$ particles in the microlayers debonded and, therefore, did not contribute to the modulus. A modified Kerner equation gave a modulus of PP with debonded particles of about 85 MPa.[32] Using this value for the modulus of the PP layers and 100 MPa for the modulus of PEO layers, the microlayer samples appeared to follow the additivity rule.

Yield strength of all of the $PP(CaCO_3)$/PEO microlayer films is shown in Figure 15(b). Although yielding was much more diffuse in the microlayer films than in the control films, the yield strength of the microlayer films followed the rule of mixtures for continuous layers in the stretch direction.

As with the $PE(CaCO_3 + SG)$/PEO microlayer films, the $PP(CaCO_3)$/PEO microlayer films showed synergistic effects in fracture strength if the microlayer contained at least 20 vol % $PP(CaCO_3)$. This improvement in fracture strength was attributed to strain hardening of PEO that was facilitated by the microlayer morphology. However, even compositions with only 10 vol % PEO exhibited enhancement in ductility, with fracture strains at least twice that of the PEO control film.

SUMMARY

The microlayer process was used to develop a tough, breathable film. Two systems were produced: one with poly(ethylene oxide) (PEO) and $CaCO_3$-filled linear low-density polyethylene, and the other with PEO and $CaCO_3$-filled polypropylene. Especially with the $PP(CaCO_3)$/PEO system, systematic variation in composition and number of layers made it possible to obtain large changes in the WVTR. Structural models based on tortuousity concepts were developed to describe water vapor transport through the microlayer films. The filled polyolefin layers were viewed as impermeable. As the number of layers increased, the polyolefin layers changed from continuous to discontinuous. The measured WVTR was well described by tortuousity models for permeability, and an effective aspect ratio of the polyolefin layers was obtained that gradually decreased as the layers became thinner. In addition to high WVTR values, the breathable films produced by microlayering PEO with a filled polyole-

fin exhibited much better toughness and ductility than PEO alone.

The authors acknowledge the generous financial support of the Kimberly-Clark Corp.

REFERENCES

1. Schrenk, W. J.; Alfrey, T. In Polymer Blends; Paul, D. R.; Newman, S., Eds.; Academic Press: New York, 1978, vol. 2.
2. Subramanian, P. M. Polym Eng Sci 1985, 25, 483.
3. Subramanian, P. M.; Mehra, V. Polym Eng Sci 1987, 27, 663.
4. Kirkpatrick, D. E.; McLemore, J. K.; Wright, M. A. J Appl Polym Sci 1992, 46, 377.
5. Lohfink, G. W.; Kamal, M. R. Polym Eng Sci 1993, 33 1404.
6. Gopalakrishnan, R.; Schultz, J. M.; Gohil, R. H. J Appl Polym Sci 1995, 56, 1749.
7. Holsti-Miettinen, R. M.; Perttilä, K P.; Seppälä, J. V.; Heino, M. T. J Appl Polym Sci 1995, 58, 1551.
8. Kamal, M. R.; Gamabi, H.; Hozhabr, S.; Arghyris, L. Polym Eng Sci 1995, 35, 41.
9. Kit, K. M.; Schultz, J. M.; Gohil, R. M.; Polym Eng Sci 1995, 35, 680.
10. Sundararaj, U.; Dori, Y.; Macosko, C. W. Polymer 1995, 36, 1957.
11. Lee, S. Y.; Kim, S. C. J Appl Polym Sci 1997, 37, 463.
12. Lee, S. Y.; Kim, S. C. J Appl Polym Sci 1998, 67, 2001.
13. Dillon, M. E. In Interpenetrating Polymer Networks; Klempner, D.; Sperling, L. H.; Utracki, L. A., Eds.; ACD Advances in Chemistry Series 239; American Chemical Society; Washington: DC, 1994.
14. Mekhilef, N.; Verhoogt, H. Polymer 1996, 37, 4069.
15. Sperling, L. H. Polymeric Multicomponent Materials; Wiley: New York, 1997, p. 44.
16. Mueller, C. D.; Nazarenko, S.; Ebeling, T.; Schuman, T.; Hiltner, A.; Baer, E. Polymer Eng Sci 1997, 37, 355.
17. Mueller, C.; Kerns, J.; Ebeling, T.; Nazarenko, S.; Hiltner, A.; Baer, E. In Polymer Process Engineering 97; Coates, P. D., Ed.; The Institute of Materials: London, 1997, p. 137.
18. Im, J.; Baer, E.; Hiltner, A. In High Performance Polymers; Baer, E.; Moet, A., Eds.; Hanser: Munich, 1991, p. 176.
19. Nakamura, S.; Okamura, K.; Mizutani, Y.; Kobunshi Ronbunshu 1991, 48, 491.
20. Nakamura, S.; Okamura, K.; Kaneko, S.; Mizutani, Y. Kobunshi Ronbunshu 1991, 48, 463.
21. Nagõ, S.; Nakamura, S.; Mizutani, Y. J Appl Polym Sci 1992, 45, 1527.
22. Nakamura, S.; Kaneko, S.; Mizutani, Y. J Appl Polym Sci 1993, 49 143.
23. Nagõ, S.; Mizutani, Y. J Appl Polym Sci 1993, 50, 1815.
24. Nagõ, S.; Mizutani, Y. J Appl Polym Sci 1998, 68, 1543.
25. Kwei, T. H.; Nishi, T.; Roberts, R. F. Macromolecules 1974, 7, 667.
26. Holdsworth, A. K.; Hourston, D. J. In Interpenetration Polymer Networks; Klempner, D.; Sperling, L. H.; Utracki, L. A., Eds.; ACS Advances in Chemistry Series 239; American Chemical Society: Washington, DC, 1994; Chapter 22.
27. Encyclopedia of Polymer Science and Technology, Wiley: New York, 1985, p. 251, vol. 6, 2nd ed.
28. Robeson, L. M.; Noshay, A.; Matzner, M.; Merriam, C. N. Angew Makromol Chem 1973, 29/30, 47.
29. Kang, Y.; Araki, K.; Iwamoto, K.; Sen, M. J Appl Polym Sci 1982, 27, 2025.
30. Nielsen, L. E. J Macromol Sci (Chem) 1967, A1, 929.
31. Roulstone, B. J.; Wilkinson, M. C.; Hearn, J. Polym Int 1992, 27, 43.
32. Ferrigno, T. H. In Handbook of Fillers for Plastics; Katz, H. S.; Milewski, J. W., Eds.; Van Nostrand Reinhold: New York, 1987, p. 34.